mater.scichina.com link.springer.com

Published online 22 July 2020 | https://doi.org/10.1007/s40843-020-1395-x
Sci China Mater 2021, 64(2): 400–407

$LiGaF_2(IO_3)_2$: A mixed-metal gallium iodate-fluoride with large birefringence and wide band gap

Jin Chen[1,2], Chun-Li Hu[1] and Jiang-Gao Mao[1,2*]

ABSTRACT **The first mixed alkali-metal gallium iodate-fluoride, namely, $LiGaF_2(IO_3)_2$, was successfully obtained under hydrothermal conditions. The structure of $LiGaF_2(IO_3)_2$ features a novel two-dimensional (2D) $[GaF_2(IO_3)_2]^-$ layer composed of $[Ga_2F_4(IO_3)_6]^{4-}$ dimers further bridged by $(IO_3)^-$ groups. $LiGaF_2(IO_3)_2$ exhibits a wide band gap of 4.33 eV, corresponding to the ultraviolet (UV) absorption edge of 230 nm. Calculations of linear optical property revealed that $LiGaF_2(IO_3)_2$ has a remarkably large birefringence of 0.181 @1064 nm and 0.206@532 nm, indicating that it is a potential birefringent material that could be used from visible to UV region. This study provides a new method for the future discovery of promising optical crystals.**

Keywords: metal iodate-fluoride, birefringent material, band gap enlargement, theoretical calculations

INTRODUCTION

The exploration of novel crystals with linear or nonlinear optical properties is of current scientific interest because of their applications in laser and optical communication industry [1–6]. Since birefringence is the modulating polarized light based on the linear optical property, birefringent crystals are able to be applied in the polarization devices [7–11]. A few commercialized birefringent crystals have been used from ultraviolet (UV) to near-infrared (NIR) region including YVO_4 [11], MgF_2 [12], α-BaB_2O_4 [13], and $CaCO_3$ [14]. Nonetheless, new and better birefringent materials are still merited further explorations with the development of theories for finding new birefringent-active units.

Generally, two types of oxide-based units with large macroscopic anisotropic mainly contribute to the birefringence: planar π-conjugated anions and second-order Jahn-Teller (SOJT) distorted cations. The former type is widely studied like metal cyanurates, borates and borate derivatives [14–22]. Cyanurates contain a considerable polarization unit with large birefringence and short absorption edge [17–22]. But their thermal stabilities are poorer than those of pure inorganic crystals. As for borates, B–O units may not be the superior birefringent genes, but strong covalent B–O bonds could induce short absorption edges and large laser-induced damage thresholds [LIDTs] [23–30]. For example, $Ca(BO_2)_2$ achieves the deep-UV absorption edge, the large birefringence, and the high LIDTs, showing that it is an excellent deep-UV birefringent material [28]. On the other hand, the SOJT cations include d^0 transition metal (TM) cations (e.g., V^{5+}, Nb^{5+}) and lone-pair cations (Bi^{3+}, Sn^{2+}). The d^0-TM-centered oxide octahedra could generate large birefringences (Δn) such as YVO_4 (Δn= 0.225@633 nm) [11]. Besides, the lone-pair cations of Sb^{3+} and Sn^{2+} could make the crucial contributions to the birefringences [5,14,24–27]. For example, $Sn_2B_5O_9Cl$ shows a large birefringence (0.168@546 nm) which is about 16 times that of $Ba_2B_5O_9Cl$ [14].

Recently, it is reported that the Se^{4+}- and I^{5+}-centered oxyanions can also make great contributions to birefringence [31–37]. For example, a series of Bi^{3+}-$(SeO_3)^{2-}$ crystals were obtained with large birefringence and the theoretical studies revealed that the contributions of the selenite groups are much larger than that of Bi^{3+} cation [33]. Moreover, the introduction of iodate groups can enlarge the birefringence in the MO_4-containing systems. However, the birefringence of $Sr[B(OH)_4](IO_3)$ (0.0536 @589.6 nm) is smaller than those of pure metal iodates [34]. The introduction of IO_3 group into metal phosphate induced an enhanced birefringence of 0.060@1064 nm in $Pb_2(IO_3)(PO_4)$, but lead to a narrower band gap of 3.89 eV owing to the existence of Pb^{2+} cation [35]. As we

[1] State Key Laboratory of Structural Chemistry, Fujian Institute of Research on the Structure of Matter, Chinese Academy of Sciences, Fuzhou 350002, China
[2] University of the Chinese Academy of Sciences, Beijing 100039, China
* Corresponding author (email: mjg@fjirsm.ac.cn)

know, the small birefringence and narrow band gap might hamper the effective application in UV region. It is reported that the introduction of F^- anions can significantly enlarges both the band gap and structural polarization of the materials [36–38]. For example, α- and β-$Ba_2[GaF_4(IO_3)_2]IO_3$ display both wide band gaps (4.61 and 4.35 eV) and large birefringences (0.126 and 0.135@1064 nm, respectively) [36]. Notably, both Ga^{3+} and F^- ions can broaden their band gaps, and the moderately distorted GaO_2F_4 octahedra (Δd=0.32 and 0.44) make some contributions to the birefringences. Such an analogous effect can be observed in $Pb_2GaF_2(SeO_3)_2Cl$ [37]. Thus, we expected that combination of the gallium oxide-fluoride octahedron with iodate groups would result in materials with both wide band gaps and excellent birefringence. Herein, our explorations on the A-Ga-F-IO_3 system successfully afford the first mixed alkali-metal gallium iodate-fluoride, namely, $LiGaF_2(IO_3)_2$, with a wide band gap (4.33 eV) and large birefringence (0.181 @1064 nm and 0.206@532 nm).

EXPERIMENTAL SECTION

Materials and methods

$LiNO_3$ (99+%), I_2O_5 (99.0%), V_2O_5 (99.0%), LiF (98%), and HF (40+%, AR) were purchased from Aladdin. Rigaku MiniFlex II diffractometer with graphite-monochromated Cu Kα radiation was used to perform powder X-ray diffraction (XRD) measurements in the 2θ range of 10°−70° with a step size of 0.02°. A field emission scanning electron microscope (FESEM, JSM6700F) with energy dispersive X-ray spectroscope (EDS, Oxford INCA) was applied to perform microprobe elemental analyses. IR spectrum was recorded on a Magna 750 FT-IR spectrometer in the form of KBr pellets in the range from 4000 to 400 cm^{-1}. Ultraviolet-visible-NIR (UV-Vis-NIR) spectrum in the range of 200−2500 nm was recorded on a PerkinElmer Lambda 950 UV-Vis-NIR spectrophotometer. Reflectance spectrum was converted into absorption spectrum by using Kubelka-Munk function [39]. Thermogravimetric analysis (TGA) and differential scanning calorimetry (DSC) studies were performed with a NETZCH STA 449F3 unit under N_2 atmosphere, at a heating rate of 10°C min^{-1} in the range of 30–1000°C.

Synthesis

Single crystals of $LiGa(IO_3)_2F_2$ were isolated *via* hydrothermal reactions. The starting materials are Ga_2O_3 (93.7 mg, 0.5 mmol), $LiNO_3$ (68.95 mg, 1 mmol), I_2O_5 (333.8 mg, 1 mmol), HF (350 μL), and H_2O (4 mL). A mixture of the starting materials was put into Teflon pouches (23 mL) sealed in an autoclave and heated at 230°C for 72 h, then cooled to 30°C at 2°C h^{-1}. Colorless brick-shaped crystals of $LiGaF_2(IO_3)_2$ were obtained in a high yield of ~80% (based on I) (Fig. 1). The elemental distribution map revealed the existence of Ga, I, and F in $LiGaF_2(IO_3)_2$ (Fig. 2).

Single-crystal structure determination

Single-crystal XRD data were collected on an Agilent Technologies SuperNova dual-wavelength CCD diffractometer with Mo Kα radiation (λ=0.71073 Å) at 293 K. Data reduction was performed with CrysAlisPro, and absorption correction based on the multi-scan method was applied [40]. The structure of $LiGaF_2(IO_3)_2$ was determined by the direct methods and refined by full-matrix least-squares using SHELXL-2014 [41]. All of the non-hydrogen atoms were refined with anisotropic thermal parameters. The structure was checked for missing symmetry elements using PLATON, and none was found [42]. Crystallographic data and structural refinements of the title compound are listed in Table 1, and selected bond distances are listed in Table S1.

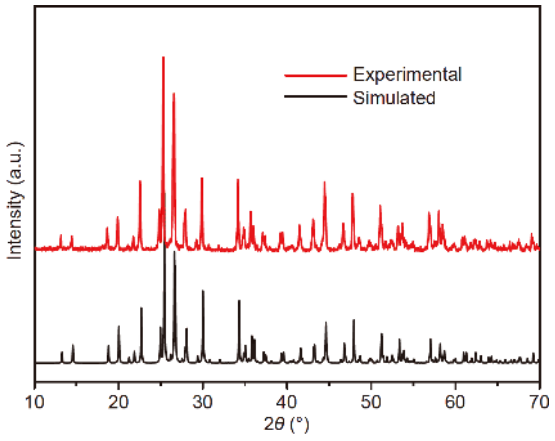

Figure 1 Simulated and measured powder XRD patterns of $LiGaF_2$-$(IO_3)_2$.

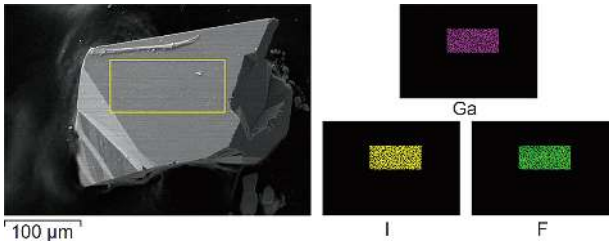

Figure 2 SEM image of $LiGaF_2(IO_3)_2$ and its elemental distribution maps.

Table 1 Crystallographic data for $LiGaF_2(IO_3)_2$

Formula	$LiGaF_2(IO_3)_2$
Formula weight	464.46
Crystal system	Monoclinic
Space group	$P2_1/n$ (No. 14)
T (K)	293(2)
a (Å)	9.9994(4)
b (Å)	5.1160(2)
c (Å)	12.6619(5)
β (°)	106.444(5)
V (Å^3)	621.25(4)
Z	4
D_c (g cm^{-3})	4.966
μ (mm^{-1})	14.397
GOF on F^2	0.979
R_1, wR_2 [$I>2\sigma(I)$]^a	0.0249, 0.0537
R_1, wR_2 (all data)^a	0.0303, 0.0582

a) $R_1=\sum||F_o|-|F_c||/\sum|F_o|$, and $wR_2=\{\sum w[(F_o)^2-(F_c)^2]^2/\sum w[(F_o)^2]^2\}^{1/2}$.

Theoretical calculations

Single-crystal structural data of $LiGaF_2(IO_3)_2$ were used for the theoretical calculations. The electronic structures and optical properties were calculated by using a plane-wave pseudopotentials method within density functional theory (DFT) implemented in the total energy code CASTEP [43,44]. For the exchange and correlation functional, Perdew-Burke-Ernzerhof (PBE) in the generalized gradient approximation (GGA) was applied [45]. The interactions between the ionic cores and the electrons were described by the norm-conserving pseudopotential [46]. The following valence-electron configurations were considered in the computation: Li $2s^1$, Ga $3d^{10}4s^24p^1$, I $5s^25p^5$, F $2s^22p^5$ and O $2s^22p^4$. The numbers of plane waves included in the basis sets were determined by cutoff energies of 850 eV. Monkhorst-Pack k-point sampling of 4×1×2 was used to perform numerical integration of the Brillouin zone. During the optical property calculations, more than 300 empty bands were involved to ensure the convergence of linear optical properties.

RESULTS AND DISCUSSION

Structural description

$LiGaF_2(IO_3)_2$ crystallized in $P2_1/n$ (No. 14) and its structure features novel two-dimensional (2D) $[GaF_2(IO_3)_4]^-$ layers separated by Li^+ ions (Fig. 3).

The asymmetric unit of $LiGaF_2(IO_3)_2$ contains one Li, one Ga, two I, two F, and six O atoms. All of them occupy the general sites. The Ga^{3+} is octahedrally coordinated by four O atoms from four different iodate groups and two F atoms, whereas both I^{5+} cations adopt the IO_3 triangular pyramidal coordination geometries. The bond lengths of 1.962(3) to 1.996(3) Å for Ga–O bonds, 1.853(3) and 1.868(3) Å for Ga–F bonds, and 1.786(3) to 1.844(3) Å for I–O bonds, are comparable to those reported in other metal gallium iodate-fluorides [36]. The GaF_2O_4 octahedron exhibits a slightly smaller distortion of Δd=0.25 than those (Δd=0.32 and 0.44) in α- and β-$Ba_2[GaF_4(IO_3)_2](IO_3)$ [36]. The Li^+ ion is octahedrally coordinated by two F atoms and four O atoms from four iodate groups with Li–O bond lengths of 2.029(9)–2.191(9) Å and Li–F bond separations of 2.007(9)–2.033(9) Å. The bond valance sum (BVS) values of 1.07, 3.08, and 4.89–4.98 for Li, Ga and I atoms indicate the oxidation states of +1, +3 and +5 for Li, Ga and I, respectively.

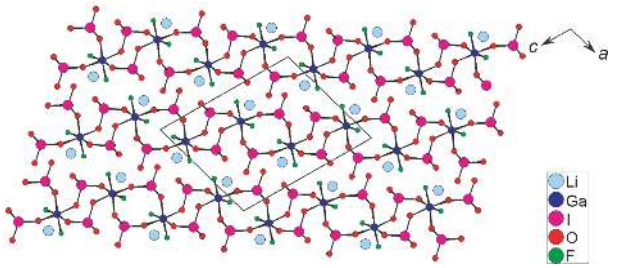

Figure 3 View of the structure of $LiGaF_2(IO_3)_2$ along b direction.

Each GaF_2O_4 octahedron links with four IO_3 groups and two *cis*-equatorial terminal F^- anions to form a 0D $[GaF_2(IO_3)_4]^{3-}$ unit (Fig. 4a). Two neighboring such units are bridged by a pair of $I(1)O_3$ groups into a $[Ga_2F_4(IO_3)_6]^{4-}$ dimer with a Ga_2I_2 4-MR (member ring) (Fig. 4b). Furthermore, each dimer links with four other neigibors *via* the briding of $I(2)O_3$ groups into a novel 2D $[GaF_2(IO_3)_2]^-$ layer parallell to the (1 0 1) plane with Ga_6I_6 12-MRs (Fig. 4c), such type of metal iodate layer has not been observed previously.

It is interesting to compare the anionic architecture in the title compound with those in α- and β-$Ba_2[GaF_4(IO_3)_2]IO_3$. Isolated metal iodate coordination anion usually forms when all of the iodate and fluoride anions adopt the unidentate fashion and such anions usually possess high negative charges as the $[GaF_4(IO_3)_2]^{3-}$ anions in α- and β-$Ba_2[GaF_4(IO_3)_2]IO_3$. In layered $[GaF_2(IO_3)_2]^-$, each iodate anion connects with two Ga atoms.

Thermal analyses

TGA show that $LiGaF_2(IO_3)_2$ is thermally stable up to 400°C (Fig. 5). The thermal behavior features one sharp

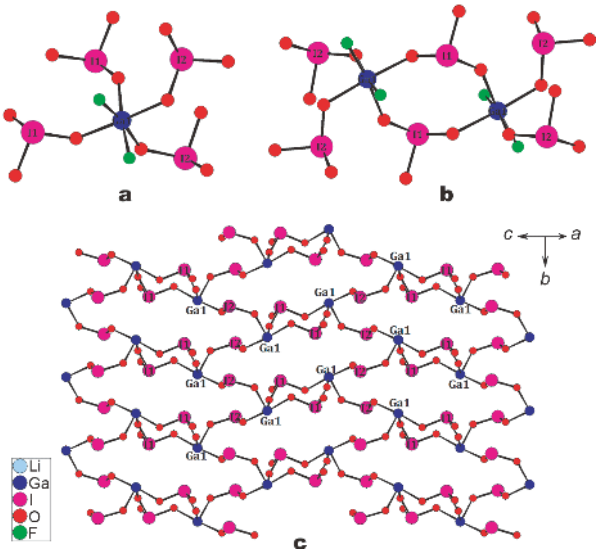

Figure 4 The feature of (a) the $[GaF_2(IO_3)_4]^{3-}$ cluster, (b) the $[Ga_2F_4(IO_3)_6]^{4-}$ dimer, and (c) the 2D $[GaF_2(IO_3)_2]^-$ layer. The unidentate F and O(6) are removed for clear.

decomposition (450–550°C) corresponding to the release of I_2, O_2 and F_2, which is consistent with the endothermic peak at 518°C in the DSC curve. The residual is expected to be $LiGaO_2$. The experimental weight loss of 72.74% is very close to the calculated value (72.68%).

Optical measurements

IR spectrum gives the vibrational bands: 759, 502, and 456 cm^{-1} (Fig. S1). The absorption peak of 759 cm^{-1} belongs to vibrational bands of Ga–O/F vibration, and the bands of 502, and 456 cm^{-1} could be assigned to I–O vibration peaks [36].

UV-Vis-IR absorption spectrum reveals that $LiGaF_2(IO_3)_2$ has a wide band gap of 4.33 eV, corresponding to its absorption edge at 230 nm (Fig. 6). Therefore, $LiGaF_2(IO_3)_2$ is a potential UV birefringent material. Significantly, such wide band gap is obviously larger than those of Bi^{3+}-, V^{5+}- and Ce^{4+}-based iodate-fluorides, such as 3.97 eV for $Bi(IO_3)F_2$ [47], 2.39 eV for $CsVO_2F(IO_3)$ [6] and 2.6 eV for $Ce(IO_3)_2F_2{\cdot}H_2O$ [48]. Hence, it is believed that both fluoride anions and blue-shift cations such as Ga^{3+} cation can widen the band gaps of metal iodates.

Structure-property relationship

Results of the band structure calculations show that $LiGaF_2(IO_3)_2$ is an indirect-band-gap compound with loose conduction band (CB) and dense valence band (VB) (Fig. S2). The theoretical band gap of $LiGaF_2(IO_3)_2$ is

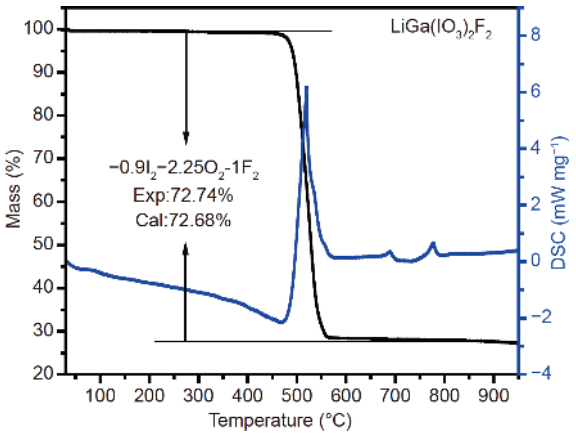

Figure 5 TGA and DSC curves of $LiGaF_2(IO_3)_2$ under N_2 atmosphere.

3.595 eV, which is much smaller than the result from the UV-Vis-IR measurement (4.33 eV). Therefore, we adopt the scissor of 0.735 eV, for matching the underestimation between the theoretical and experimental values.

The partial density of states (PDOS) graph of $LiGaF_2(IO_3)_2$ was shown in Fig. 7. The highest VB is determined by the O 2p nonbonding orbitals, whereas the empty O 2p and I 5p states majorly contribute to the lowest CB. Importantly, the orbitals of the blue-shift elements (Li, Ga and F) show no obvious contributions to the band gap, which is also observed in α- and β-$Ba_2[GaF_4(IO_3)_2]IO_3$ [36]. Besides, in the Bi^{3+}-, V^{5+}- and Ce^{4+}-based iodate-fluorides, the cations' states clearly decrease the lowest CB and further induce the smaller band gaps. Therefore, it is deemed that the band gap engineering follows these rules: (1) the orbitals of IO_3 groups define the highest VB and lowest CB; (2) the

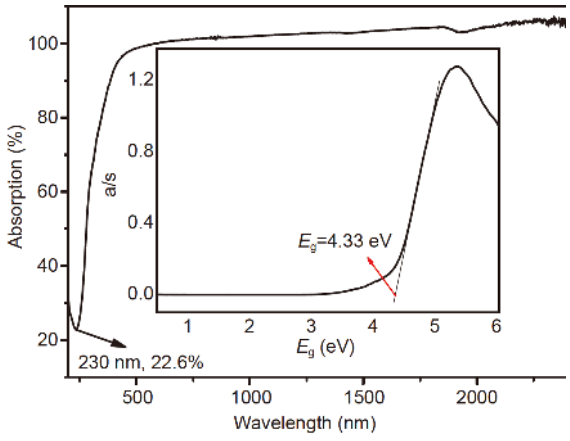

Figure 6 UV-Vis-IR spectrum of $LiGaF_2(IO_3)_2$. The inset shows the band gap of $LiGaF_2(IO_3)_2$. a/s: absorption coefficient/scattering coefficient.

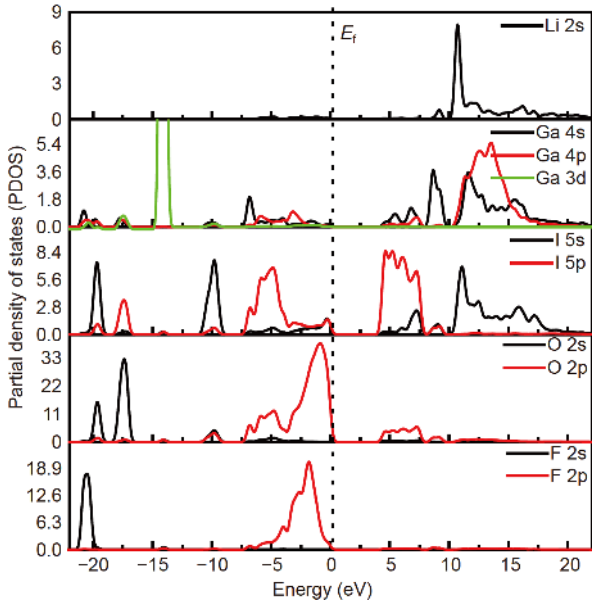

Figure 7 The scissor-added PDOS for $LiGaF_2(IO_3)_2$.

orbitals of blue-shift cations locate at higher levels than the empty I 5p and O 2p in CB region; (3) F 2p orbitals locate at the lower level than the occupied O 2p in VB.

We also studied the linear optical property *via* the calculation complex dielectric function:

$$\varepsilon(\omega) = \varepsilon_1(\omega) + i\varepsilon_2(\omega),$$

where $\varepsilon_1(\omega)$ is the real part and $\varepsilon_2(\omega)$ is the imaginary part. As shown in Fig. 8a, the largest absorption is 5.66 eV for the averaged imaginary part, which can be attributed to the electronic inter-band transitions from O 2p orbitals to I 5d and the empty Ga 3d orbitals. And the $\varepsilon(0)$ represents the average static dielectric constant, which is 3.96 from the averaged real part. The dispersion curves of refractive indices display strong anisotropy (Fig. 8b), which was calculated by

$$n^2(\omega) = \varepsilon(\omega),$$

where $n(\omega)$ is the refractive index and $\varepsilon(\omega)$ is the complex dielectric function. Thus, the birefringence of $LiGaF_2(IO_3)_2$ was calculated to be 0.181@1064 nm. Indeed, $LiGaF_2(IO_3)_2$ realizes better balance between the band gap and birefringence than the reported typical metal iodates (Table 2). Moreover, the remarkably high birefringence of 0.206@532 nm indicates that $LiGaF_2(IO_3)_2$ is a competitive UV birefringent material to the commercial α-BaB_2O_4 (0.11) [8] and $CaCO_3$ (0.16) [13].

We investigated the electron density difference map for determining the origin of the large birefringence. Fig. 9 displays that the entire electron density around the I–O, Ga–O, and Ga–F bonds was anisotropically polarized, indicating the strong covalent bonding characteristics of these three types of bonds. Hence, we deem that both IO_3 and GaO_4F_2 polyhedra contribute to the large birefringence of $LiGaF_2(IO_3)_2$.

CONCLUSIONS

$LiGaF_2(IO_3)_2$ was rationally designed *via* combining gallium oxide-fluoride octahedron with iodate groups in the alkali metal system firstly. The structure of $LiGaF_2(IO_3)_2$ features a novel 2D $[GaF_2(IO_3)_2]^-$ layer built from GaO_4F_2 polyhedra interconnected by bridging iodate anions. It exhibits a large band gap of 4.33 eV, a wide transmittance window of 0.23–9.37 μm, and high thermal stability of >400°C. Furthermore, theoretical studies revealed that IO_3 groups defined the band gap, but the blue-shift ions (Li^+, Ga^{3+} and F^-) could widen the band gap. The calculated birefringence is as high as 0.181@1064 nm and 0.206@532 nm. Hence, $LiGaF_2(IO_3)_2$ is a promising UV birefringent material. Results of our study indicate that

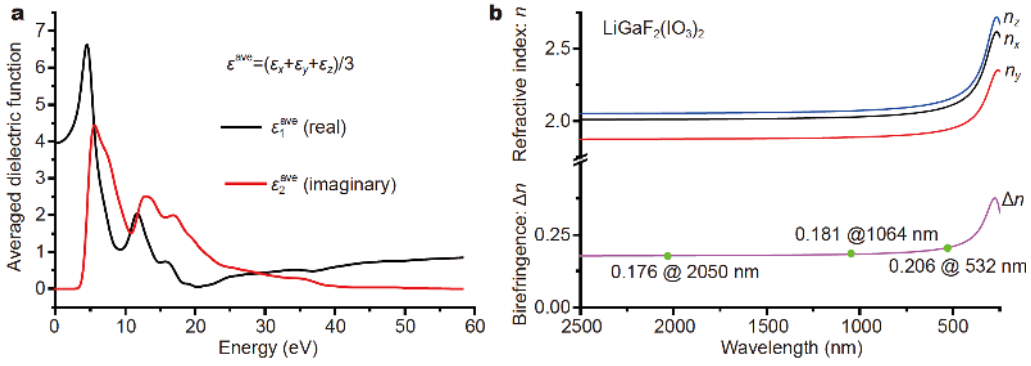

Figure 8 (a) Calculated average imaginary part and real part of the dielectric function of $LiGaF_2(IO_3)_2$, and (b) the calculated refractive indices for $LiGaF_2(IO_3)_2$.

Table 2 Band gap and birefringence @1064 nm for typical metal iodates

Compounds	Band gap (eV)	Birefringence	Refs.
$Bi(IO_3)F_2$	3.97	0.209	[47]
α-$Ba_2[GaF_4(IO_3)_2]IO_3$	4.61	0.126	[36]
β-$Ba_2[GaF_4(IO_3)_2]IO_3$	4.35	0.135	[36]
$ZnFIO_3$	4.20	0.194	[38]
$Sr[B(OH)_4](IO_3)$	4.42	0.0536[a]	[34]
$Pb_2(IO_3)(PO_4)$	3.89	0.060	[35]
$LiGaF_2(IO_3)_2$	4.35	0.181	This work

a) The value was measured at 589.6 nm.

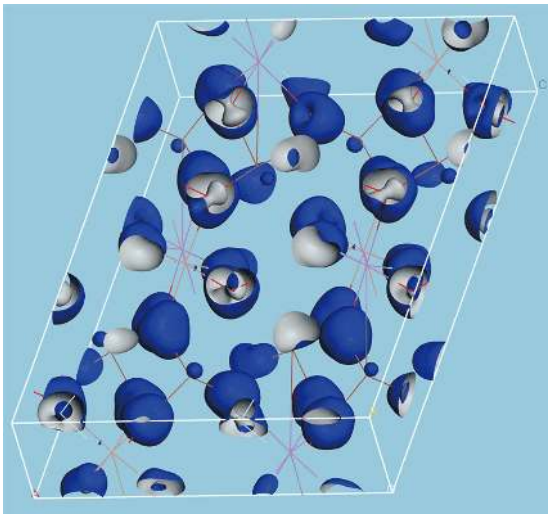

Figure 9 The electron density difference map of $LiGaF_2(IO_3)_2$.

the iodate unit is an excellent birefringent gene, and its combination with blue-shift ions could lead to materials with wide band gaps and large birefringence. Further investigations into UV metal iodates with commendable linear or nonlinear optical properties are underway.

Received 14 April 2020; accepted 15 May 2020; published online 22 July 2020

1 Ok KM, Chi EO, Halasyamani PS. Bulk characterization methods for non-centrosymmetric materials: Second-harmonic generation, piezoelectricity, pyroelectricity, and ferroelectricity. Chem Soc Rev, 2006, 35: 710–717
2 Xia Z, Poeppelmeier KR. Chemistry-inspired adaptable framework structures. Acc Chem Res, 2017, 50: 1222–1230
3 Mutailipu M, Zhang M, Yang Z, *et al.* Targeting the next generation of deep-ultraviolet nonlinear optical materials: Expanding from borates to borate fluorides to fluorooxoborates. Acc Chem Res, 2019, 52: 791–801
4 Yang Y, Wu K, Zhang B, *et al.* Infrared nonlinear optical polymorphs α- and β-$SrCu_2SnS_4$ exhibiting large second harmonic generation responses with requisite phase-matching behavior. Chem Mater, 2020, 32: 1281–1287
5 Han S, Mutailipu M, Tudi A, *et al.* $PbB_5O_7F_3$: A high-performing short-wavelength nonlinear optical material. Chem Mater, 2020, 32: 2172–2179
6 Chen J, Hu CL, Zhang XH, *et al.* $CsVO_2F(IO_3)$: An excellent SHG material featuring an unprecedented 3D $[VO_2F(IO_3)]^-$ anionic framework. Angew Chem Int Ed, 2020, 59: 5381–5384
7 Weber MF, Stover CA, Gilbert LR, *et al.* Giant birefringent optics in multilayer polymer mirrors. Science, 2000, 287: 2451–2456
8 Zhou GQ, Xu J, Chen XD, *et al.* Growth and spectrum of a novel birefringent α-BaB_2O_4 crystal. J Cryst Growth, 1998, 191: 517–519
9 Xie ZY, Sun LG, Han GZ, *et al.* Optical switching of a birefringent photonic crystal. Adv Mater, 2008, 20: 3601–3604
10 Wu B, Tang D, Ye N, *et al.* Linear and nonlinear optical properties of the $KBe_2BO_3F_2$ (KBBF) crystal. Opt Mater, 1996, 5: 105–109
11 Luo HT, Tkaczyk T, Dereniak EL, *et al.* High birefringence of the yttrium vanadate crystal in the middle wavelength infrared. Opt Lett, 2006, 31: 616–618
12 Dodge MJ. Refractive properties of magnesium fluoride. Appl Opt, 1984, 23: 1980–1985
13 Ghosh G. Dispersion-equation coefficients for the refractive index and birefringence of calcite and quartz crystals. Opt Commun, 1999, 163: 95–102
14 Guo J, Tudi A, Han S, *et al.* $Sn_2B_5O_9Cl$: A material with large birefringence enhancement activated prepared *via* alkaline-earth-metal substitution by tin. Angew Chem Int Ed, 2019, 58: 17675–17678
15 Chen X, Zhang B, Zhang F, *et al.* Designing an excellent deep-ultraviolet birefringent material for light polarization. J Am Chem Soc, 2018, 140: 16311–16319
16 Wang Z, He J, Hu B, *et al.* $Ca_2B_5O_9Cl$ and $Sr_2B_5O_9Cl$: Nonlinear optical crystals with deep-ultraviolet transparency windows. ACS Appl Mater Interfaces, 2020, 12: 4632–4637
17 Kang K, Liang F, Meng X, *et al.* $Ba_2M(C_3N_3O_3)_2$ (M=Sr, Pb): Band engineering from p-π interaction *via* homovalent substitution in metal cyanurates containing planar π-conjugated groups. Inorg Chem, 2019, 58: 9553–9556
18 Wang N, Liang F, Yang Y, *et al.* A new ultraviolet transparent hydra-cyanurate $K_2(C_3N_3O_3H)$ with strong optical anisotropy from delocalized π-bonds. Dalton Trans, 2019, 48: 2271–2274
19 Song Y, Lin D, Luo M, *et al.* $RbNa(HC_3N_3O_3)\cdot 2H_2O$ exhibiting a strong second harmonic generation response and large birefringence as a new potential UV nonlinear optical material. Inorg Chem Front, 2020, 7: 150–156
20 Tang J, Meng X, Liang F, *et al.* Structural diversity and giant bi-

refringence in cyanates BaCNOX (X=Cl, Br, I, and CNO) containing linear π-conjugated units: A combined experimental and theoretical study. Cryst Growth Des, 2020, 20: 1242–1247
21 Lu J, Lian YK, Xiong L, *et al.* How to maximize birefringence and nonlinearity of π-conjugated cyanurates. J Am Chem Soc, 2019, 141: 16151–16159
22 Lin D, Luo M, Lin C, *et al.* $KLi(HC_3N_3O_3)\cdot 2H_2O$: Solvent-drop grinding method toward the hydro-isocyanurate nonlinear optical crystal. J Am Chem Soc, 2019, 141: 3390–3394
23 Chen C, Ye N, Lin J, *et al.* Computer-assisted search for nonlinear optical crystals. Adv Mater, 1999, 11: 1071–1078
24 Schönegger S, Pielnhofer F, Saxer A, *et al.* Synthesis and characterization of the tin iodide borate $Sn_3[B_3O_7]I$. Inorg Chem, 2019, 58: 6088–6094
25 Schönegger S, Jantz SG, Saxer A, *et al.* Synthesis and characterization of the first tin fluoride borate $Sn_3[B_3O_7]F$ with second harmonic generation response. Chem Eur J, 2018, 24: 16036–16043
26 Yang Y, Qiu Y, Gong P, *et al.* Lone-pair enhanced birefringence in an alkaline-earth metal tin(II) phosphate $BaSn_2(PO_4)_2$. Chem Eur J, 2019, 25: 5648–5651
27 Huang C, Zhang F, Cheng S, *et al.* α-, β-$Pb_4B_2O_7$ and α-, β-$Pb_4B_6O_{13}$: Polymorphism drives changes in structure and performance. Sci China Mater, 2020, 63: 806–815
28 Liu H, Wang Y, Zhang B, *et al.* $CsAlB_3O_6F$: A beryllium-free deep-ultraviolet nonlinear optical material with enhanced thermal stability. Chem Sci, 2020, 11: 694–698
29 Xie Z, Wang Y, Cheng S, *et al.* Synthesis, characterization, and theoretical analysis of three new nonlinear optical materials $K_7MRE_2B_{15}O_{30}$ (M=Ca and Ba, RE=La and Bi). Sci China Mater, 2019, 62: 1151–1161
30 Yang Z, Tudi A, Lei BH, *et al.* Enhanced nonlinear optical functionality in birefringence and refractive index dispersion of the deep-ultraviolet fluorooxoborates. Sci China Mater, 2020, 63: 1480–1488
31 Huang J, Guo S, Zhang Z, *et al.* Designing excellent mid-infrared nonlinear optical materials with fluorooxo-functional group of d^0 transition metal oxyfluorides. Sci China Mater, 2019, 62: 1798–1806
32 Wang XX, Li XB, Hu CL, *et al.* $Ag_4Hg(SeO_3)_2(SeO_4)$: A novel SHG material created in mixed valent selenium oxides by *in situ* synthesis. Sci China Mater, 2019, 62: 1821–1830
33 Gong YP, Hu CL, Kong F, *et al.* Exploration of new birefringent crystals in bismuth d^0 transition metal selenites. Chem Eur J, 2019, 25: 3685–3694
34 Peng G, Lin C, Zhao D, *et al.* $Sr[B(OH)_4](IO_3)$ and $Li_4Sr_5[B_{12}O_{22}(OH)_4](IO_3)_2$: Two unprecedented metal borate-iodates showing a subtle balance of enlarged band gap and birefringence. Chem Commun, 2019, 55: 11139–11142
35 Zhang XH, Yang BP, Chen J, *et al.* A new iodate-phosphate $Pb_2(IO_3)(PO_4)$ achieving great improvement in birefringence activated by $(IO_3)^-$ groups. Chem Commun, 2020, 56: 635–638
36 Chen J, Hu CL, Mao FF, *et al.* A facile route to nonlinear optical materials: Three-site aliovalent substitution involving one cation and two anions. Angew Chem Int Ed, 2019, 58: 2098–2102
37 You F, Liang F, Huang Q, *et al.* $Pb_2GaF_2(SeO_3)_2Cl$: Band engineering strategy by aliovalent substitution for enlarging bandgap while keeping strong second harmonic generation response. J Am Chem Soc, 2019, 141: 748–752
38 Gai M, Wang Y, Tong T, *et al.* $ZnIO_3F$: Zinc iodate fluoride with large birefringence and wide band gap. Inorg Chem, 2020, 59: 4172–4175
39 Kubelka P, Munk F. An article on optics of paint layers. Z Technol Phys, 1931, 12: 886–892
40 Blessing RH. An empirical correction for absorption anisotropy. Acta Crystlogr A Found Crystlogr, 1995, 51: 33–38
41 Sheldrick GM. Crystal structure refinement with *SHELXL*. Acta Crystlogr C Struct Chem, 2015, 71: 3–8
42 Spek AL. Single-crystal structure validation with the program *PLATON*. J Appl Crystlogr, 2003, 36: 7–13
43 Milman V, Winkler B, White JA, *et al.* Electronic structure, properties, and phase stability of inorganic crystals: A pseudopotential plane-wave study. Int J Quant Chem, 2000, 77: 895–910
44 Segall MD, Lindan PJD, Probert MJ, *et al.* First-principles simulation: Ideas, illustrations and the CASTEP code. J Phys-Condens Matter, 2002, 14: 2717–2744
45 Perdew JP, Burke K, Ernzerhof M. Generalized gradient approximation made simple. Phys Rev Lett, 1996, 77: 3865–3868
46 Lin JS, Qteish A, Payne MC, *et al.* Optimized and transferable nonlocal separable *ab initio* pseudopotentials. Phys Rev B, 1993, 47: 4174–4180
47 Mao FF, Hu CL, Xu X, *et al.* $Bi(IO_3)F_2$: The first metal iodate fluoride with a very strong second harmonic generation effect. Angew Chem Int Ed, 2017, 56: 2151–2155
48 Abudouwufu T, Zhang M, Cheng S, *et al.* $Ce(IO_3)_2F_2\cdot H_2O$: The first rare-earth-metal iodate fluoride with large second harmonic generation response. Chem Eur J, 2019, 25: 1221–1226

Acknowledgements This work was supported by the National Natural Science Foundation of China (21875248, 21921001, and 21975256), the Strategic Priority Research Program of the Chinese Academy of Sciences (XDB20000000), and the 100 Talents Project of Fujian Province.

Author contributions Chen J designed and engineered the samples and performed the experimental data analysis; Chen J and Hu CL performed the theoretical data analysis; Chen J wrote the paper with support from Mao JG. All authors contributed to the general discussion.

Conflict of interest The authors declare that they have no conflict of interest.

Supplementary information Supporting data are available in the online version of the paper.

Jin Chen received his BSc degree in materials science and engineering from China University of Mining and Technology (CUMT) in 2016. He then joined Professor Jiang-Gao Mao's research group as a PhD candidate at the University of Chinese Academy of Sciences (UCAS). He is currently focusing on iodate-based inorganic crystals.

Jiang-Gao Mao received his PhD from Chang-Chun Institute of Applied Chemistry, Chinese Academy of Sciences under the supervision of Professor Jiazuan Ni (Academician). He did post-doctoral research at Fujian Institute of Research on the Structure of Matter (FJIRSM), Chinese University of Hong Kong, University of Houston and Texas A&M University from 1994 to 2002. Since 2002, he has been working as a full professor at FJIRSM, CAS. His current research interest includes the design, syntheses, and crystal structures of new functional inorganic solid crystals.

$LiGaF_2(IO_3)_2$：同时展现出优异的双折射率和宽带隙的新型碘酸盐氟化物晶体

陈瑾[1,2]，胡春丽[1]，毛江高[1,2*]

摘要 本文中，我们通过水热合成得到了首例混合碱金属镓碘酸盐氟化物，即$LiGaF_2(IO_3)_2$，其晶体结构中包含了一种新型的二维阴离子层，即$[GaF_2(IO_3)_2]^-$层．该二维层是由$[Ga_2F_4(IO_3)_6]^{4-}$二聚体通过碘酸根基团进一步桥连而得的．$LiGaF_2(IO_3)_2$具有4.33 eV的宽带隙和230 nm的紫外截止边．线性光学性质计算结果表明其具有优异的双折射率，分别为0.186@1064 nm以及0.206@532 nm，这表明在可见到紫外波段，$LiGaF_2(IO_3)_2$是潜在的双折射材料．理论计算表明，Ga-O/F八面体对该晶体的带隙和双折率都起到了增强的作用．这项工作对于未来探索性能优异的光学晶体提供了新方法．

